

Fabrication of p-type ZnSe:Sb nanowires for high-performance ultraviolet light photodetector application

This article has been downloaded from IOPscience. Please scroll down to see the full text article.

2013 Nanotechnology 24 095603

(<http://iopscience.iop.org/0957-4484/24/9/095603>)

View [the table of contents for this issue](#), or go to the [journal homepage](#) for more

Download details:

IP Address: 61.132.138.217

The article was downloaded on 23/02/2013 at 00:31

Please note that [terms and conditions apply](#).

Fabrication of p-type ZnSe:Sb nanowires for high-performance ultraviolet light photodetector application

Biao Nie¹, Lin-Bao Luo¹, Jing-Jing Chen¹, Ji-Gang Hu¹, Chun-Yan Wu¹, Li Wang¹, Yong-Qiang Yu¹, Zhi-Feng Zhu¹ and Jian-Sheng Jie²

¹ School of Electronic Science and Applied Physics, Hefei University of Technology, Hefei, Anhui 230009, People's Republic of China

² Institute of Functional Nano and Soft Materials (FUNSOM) and Jiangsu Key Laboratory for Carbon-Based Functional Materials and Devices, Soochow University, Suzhou, Jiangsu 215123, People's Republic of China

E-mail: luolb@hfut.edu.cn


Received 17 November 2012, in final form 19 January 2013

Published 12 February 2013

Online at stacks.iop.org/Nano/24/095603

Abstract

p-type ZnSe nanowires (NWs) with tunable electrical conductivity were fabricated on a large scale by evaporating a mixed powder composed of ZnSe and Sb in different ratios. According to the structural characterization, the Sb-doped ZnSe NWs are of single crystalline form and grow along the [001] direction. The presence of Sb in the ZnSe NWs was confirmed by XPS spectra. Electrical measurement of a single ZnSe:Sb NW based back-gate metal–oxide field-effect-transistor reveals that all the doped NWs exhibit typical p-type conduction characteristics, and the conductivity can be tuned over eight orders of magnitude, from $6.36 \times 10^{-7} \text{ S cm}^{-1}$ for the undoped sample to $\sim 37.33 \text{ S cm}^{-1}$ for the heavily doped sample. A crossed p–n nano-heterojunction photodetector made from the as-doped nanostructures displays pronounced rectification behavior, with a rectification ratio as high as 10^3 at $\pm 5 \text{ V}$. Remarkably, it exhibits high sensitivity to ultraviolet light illumination with good reproducibility and quick photoresponse. Finally, the work mechanism of such a p–n junction based photodetector was elucidated. The generality of the above result suggests that the as-doped p-type ZnSe NWs will find wide application in future optoelectronics devices.

 Online supplementary data available from stacks.iop.org/Nano/24/095603/mmedia

(Some figures may appear in colour only in the online journal)

1. Introduction

Recently, one-dimensional (1D) inorganic semiconductor nanostructures (e.g., nanowires, nanorods, nanoribbons, nanotubes, etc) have attracted great scientific and technical interest due to their unique optical, mechanical, chemical and optoelectronic properties relative to their thin film and bulk counterparts [1–3]. Considerable effort has been made with respect to the fabrication of various nanostructured semiconductors such as group IV (Si, Ge) [4, 5], group III–VI (GaN, GaAs) [6, 7], group II–VI (ZnSe, CdTe) [8, 9] and group VI (Se, Te) [10, 11] via chemical vapor deposition,

wet chemical routes and template-assisted methods [12]. On the basis of these nanostructures, a great many nano-optoelectronic devices including light-emitting diodes (LEDs), visible or ultraviolet light photodetectors (UVPD), logic circuits, chemical or biological sensors and solar cells with exceptionally high performance have been fabricated [13–15].

Amongst the various semiconductors mentioned above, II–VI group nanostructures have received special research interest [16, 17]. For example, zinc selenide (ZnSe), with a direct band gap of $E_g = 2.7 \text{ eV}$ at room temperature, has been extensively investigated as a candidate for blue

light-emitting diodes and blue lasers for a long time [18, 19]. Like other II–VI semiconductor nanostructures, a key feature of ZnSe NWs that has enabled much of their success has been the growth of materials with controllable electrical properties. By doping with metal elements (e.g. Cl and Ga), namely incorporating metal atoms into their crystal lattice, ZnSe nanowires with tunable electron concentrations have been successfully synthesized [20–22]. Unfortunately, due to the strong self-compensation effect and Fermi level pinning effect [23], p-type doping of ZnSe nanostructures, in particular low resistive ZnSe nanostructures with controllable electrical properties, is very difficult and remains unresolved [24, 25]. Undeniably, this difficulty has constituted the main obstacle to the development of ZnSe based optoelectronic nanodevices. Herein, we report the fabrication of highly conductive p-type ZnSe nanowires with tunable Sb doping levels for crossed high performance UVPD application. Structural characterization of the ZnSe:Sb nanowires reveals typical single-crystal nature, with a growth direction along [001]. Electrical property analysis of field effect transistors (FETs) assembled from single nanowires reveals that the conductivity of the p-type ZnSe NWs can be readily tuned over eight orders of magnitude. A crossed p–n junction device made from the as-prepared nanostructures shows pronounced current rectification behavior, with a rectification ratio as great as 10^3 at ± 5 V. Moreover, it also exhibits high sensitivity to visible light illumination with good reproducibility and quick response. The working mechanism of this new type of UVPD is finally elucidated.

2. Experiment

2.1. Synthesis of ZnSe:Sb and ZnO:Ga nanowires

The ZnSe:Sb NWs were synthesized by using ZnSe powder (Aldrich Co., 99.99%) and antimony (Sb) powder (Aldrich Co., 99.99%) as the source material and the p-type dopant, respectively. In a typical experiment, a mixture of ZnSe and Sb powder (0.2 g) was loaded into an alumina boat and transferred to the central region of a horizontal quartz tube furnace. Si substrates coated with 10 nm Au catalyst were then placed down-stream, ~ 10 cm from the evaporation source. A constant H_2 (5% in Ar) gas flow of 30 standard-state cubic centimeters per minute (sccm) was fed and the pressure in the tube was kept at 200 Torr throughout the growth process. The evaporation source was heated up to 1000°C and maintained at this temperature for 1 h. After growth, the system was cooled down to room temperature and the Si substrates with a layer of yellow wool-like product were taken out of the furnace. In this work, in total three samples with varied Sb doping levels were synthesized and marked as samples 1, 2 and 3, corresponding to the increasing antimony powder mixture to ZnSe mass ratio of 0.5%, 5% and 10%, respectively. The synthesis of the ZnO:Ga NWs in this study was achieved by using a vapor phase transport process which has been reported previously [26].

2.2. Structural characterization

The phase, morphology and crystal structure of the antimony doped ZnSe nanowires were characterized using an x-ray diffractor (XRD, Rigaku D/Max- γ B with Cu $K\alpha$ radiation), field effect scanning electron microscopy (FESEM, Philips XL 30 GEG) and high-resolution transmission electron microscopy (HRTEM, CM 200 FEG, operated at 200 kV) equipped with selected area electron diffraction (SAED). The chemical composition of the product was analyzed by x-ray photoemission spectroscopy (XPS) which was performed on a VG ESCALAB 220i-XL surface analysis system equipped with a monochromatic Al x-ray (1486.6 eV) source. PL analysis was performed on a Fluorolog3-TAU-P at room temperature with an excitation wavelength of 325 nm.

2.3. Device fabrication and characterization

Single NW based field-effect transistors (FETs) were fabricated for electrical property analysis. Briefly, the NWs were first dispersed on a SiO_2 (300 nm)/ p^+ -Si substrate with the desired density. Then, two parallel Au (70 nm) source and drain electrodes were defined by photolithography and an electron-beam evaporation method. Finally, the remaining photoresist was removed by a simple lift-off process. During device analysis, the deposited metal electrodes served as source and drain, while the p^+ -Si substrate served as the global back gate. To fabricate the crossed p-ZnSe NW/n-ZnO:Ga NW junction device, ZnO:Ga NWs were firstly dispersed on a SiO_2 (300 nm)/ p^+ -Si substrate with the desired density. Then, two Ti electrodes (70 nm) connecting the NWs were fabricated by photolithography and a metal evaporation process. Replication of this process vertical to the ZnO NWs leads to the formation of a crossed p–n junction diode. To analyze the photoresponse of the device, monochromatic UV light with wavelength of 365 nm from a Hg lamp was focused and guided onto the sample perpendicularly. All the electrical measurements were performed at room temperature using a semiconductor characterization system (Keithley 4200-SCS).

3. Results and discussion

The as-collected ZnSeNWs on Si wafer were directly transferred into an SEM chamber for morphology study. Figures 1(a)–(c) show the representative FESEM images of samples 1, 2 and 3, respectively, from which we can see that the products are largely composed of wire-like fibers with lengths of tens of micrometers, and no apparent contaminants or impurities are visualized. Figure 1(d) shows a typical TEM image of an NW with a diameter of ~ 200 nm. The corresponding lattice resolved image from HRTEM (figure 2(c)) reveals a d -spacing value of 0.67 nm, in good accordance with the c lattice constant of ZnSe. This growth direction along [001] was further confirmed by the selected area electron diffraction (SAED) pattern. Figure 1(f) depicts the typical XRD patterns of both intrinsic and Sb-doped ZnSeNWs, in which all of the diffraction peaks could be assigned to wurtzite ZnSe (JCPDS No. 80-0008) and no

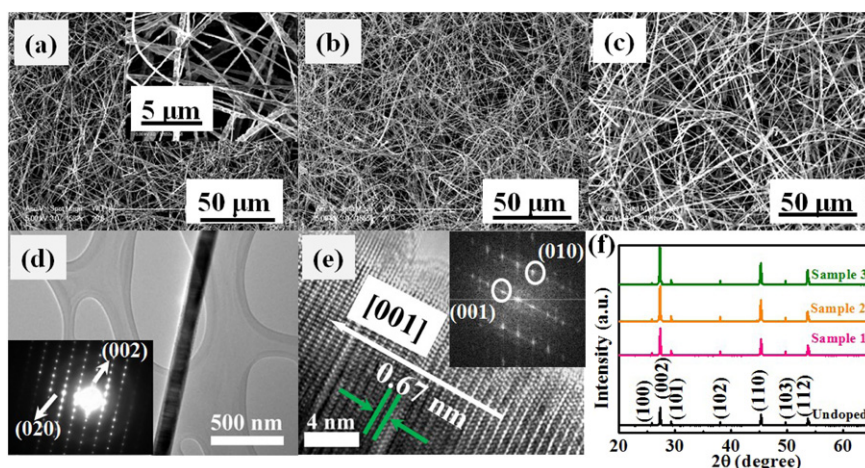


Figure 1. SEM images of ZnSe nanowires with different Sb doping levels: (a) sample 1, (b) sample 2 and (c) sample 3. (d) A typical TEM image of an individual ZnSe nanowire from sample 3; the inset shows the corresponding SAED pattern. (e) HRTEM image of the ZnSe:Sb NW; the inset shows the fast Fourier transform (FFT) pattern. (f) The XRD patterns of the undoped and doped ZnSe NWs.

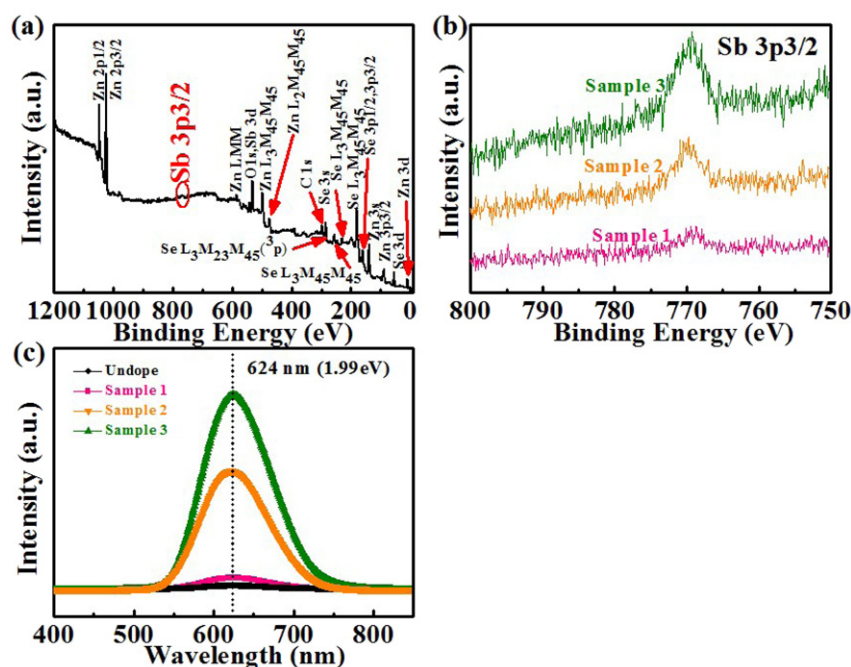


Figure 2. (a) The XPS survey spectrum of ZnSe:Sb NWs (sample 1). (b) The Sb $3p_{3/2}$ spectra of ZnSe nanowires with different doping levels. (c) PL spectra of both undoped and Sb-doped ZnSe NWs.

impurity peaks were observed, indicating the high phase purity of the products. In addition, the diffraction peaks of the Sb-doped ZnSe NWs do not show obvious peak broadening or peak shift compared with the standard ZnSe single-crystal structure, suggesting that the introduction of impurity atoms into the crystal lattice hardly influences the crystal quality of the NWs.

The incorporation of Sb atoms into the ZnSe NWs was checked by the XPS analysis. Figure 2(a) shows a typical XPS survey spectrum of sample 1, in which four typical peaks located at 285, 532.5, 55.5 and 1022 eV due to C 1s, O 1s, Se 3d and Zn 2p, respectively, are observed. As is often seen in other nanostructures, the presence of oxygen and carbon is

attributable to surface adsorption and, as usual, its influence can be omitted. It should be noted that the binding energies (BEs) of O 1s and Sb 4d, the characteristic peak of the Sb atom, happen to be almost identical. Thus, the Sb 3p, as opposed to Sb 4d, was scanned individually to further quantify the doping level. Figure 2(b) shows the spectrum of Sb $3p_{3/2}$ from the three Sb-doped samples. The Sb contents in the ZnSe NWs (samples 1, 2 and 3) are estimated to be 0.2%, 1.2% and 2.3% (wt%) from the XPS spectrum, respectively. Figure 2(c) depicts the PL spectra of the ZnSeNWs, excited by the beam of a 325 nm laser at an excitation power of 100 mW. It is obvious that a dominant emission band ascribable to the deep level (DL) emission of ZnSe at 624 nm (1.99 eV) is observed

for all of the samples. Remarkably, the DL emission becomes stronger upon Sb doping, which is probably due to increasing DL defects, such as nonstoichiometric defects and/or stacking faults and dislocations [27, 28].

To compare the electrical conduction of the as-doped ZnSe nanowires, I - V analysis of single NWs was carried out. In this study, Cu/Au metal was chosen as the electrode material as it can form good contact with nominal contact resistance [29]. Figure 3(a) depicts the typical I - V curves measured from the samples with different doping levels. The ideal linearity of the I - V curves confirms the Ohmic contact between the ZnSe:Sb NWs and the Cu/Au electrodes. Significantly, it is found that the introduction of Sb atoms can greatly increase the electrical conductivity of the ZnSe NWs. The conductivity of undoped NWs is as low as $6.36 \times 10^{-7} \text{ S cm}^{-1}$, virtually electrically insulative for electron transport. However, the conductivity increases dramatically to $\sim 0.280 \text{ S cm}^{-1}$ for sample 1, to $\sim 3.32 \text{ S cm}^{-1}$ for sample 2 and to $\sim 37.3 \text{ S cm}^{-1}$ for sample 3. To check the reproducibility of this doping method, similar electrical characterization on 40 NWs (10 NWs for each sample) was performed. The results are summarized in figure 3(b). Basically, most of the slightly doped NWs (sample 1) show conductivities between 10^{-2} and $10^{-1} \text{ S cm}^{-1}$. For sample 2, most NWs have a conductivity value in the range of 1 – 10 S cm^{-1} . For the heavily doped samples (sample 3), the conductivity values fall in the range of 10^1 – 10^2 S cm^{-1} . Remarkably, for all the samples, the conductivities are characterized by a narrow distribution.

Next, a back-Gate semiconductor field-effect transistor (FET) based on an individual ZnSe NW was fabricated to study the electrical transport properties of the Sb-doped ZnSe NWs (figure 4(a)). Figure 4(b) shows the electrical characteristics of a representative ZnSe NW FET fabricated from sample 1. The source-drain current (I_{DS}) versus source-drain voltage (V_{DS}) curves were measured under a varied gate voltage (V_G) from $+40$ to -40 V at steps of 40 V . It is noted that the device exhibits an apparent p-type gating effect; that is, when V_G decreases (increases), the conductance increases (decreases) correspondingly. The inset of figure 4(b) shows the corresponding transfer curves at 5 V . The turn-on threshold voltage is derived to be 42 V by fitting the linear part of the I_{DS} - V_G curve. Assuming a cylinder on an infinite plate model for the ZnSe NW based FET, the channel capacitance can be described by the formula $C = 2\pi\epsilon_0\epsilon_{\text{SiO}_2}L/\cos^{-1}(t/h)$, where t , L , r , d , t and ϵ_{SiO_2} represent the distance between the substrate and the center of the NW (300 nm), the channel length of the NW ($\sim 5 \mu\text{m}$), the radius of the ZnSe NW ($\sim 100 \text{ nm}$) and the dielectric constant of SiO_2 (3.9), respectively. Furthermore, the μ_h can be further estimated from the channel transconductance (g_m) of the nano-FET by using the following equation:

$$\mu_h = g_m L^2 / C V_{DS}. \quad (1)$$

Based on these values, a hole mobility of $\sim 3.18 \times 10^{-2} \text{ cm}^2 \text{ V}^{-1} \text{ s}^{-1}$ for NWs from sample 1 is obtained. In addition, the hole concentration is estimated to be $5.50 \times$

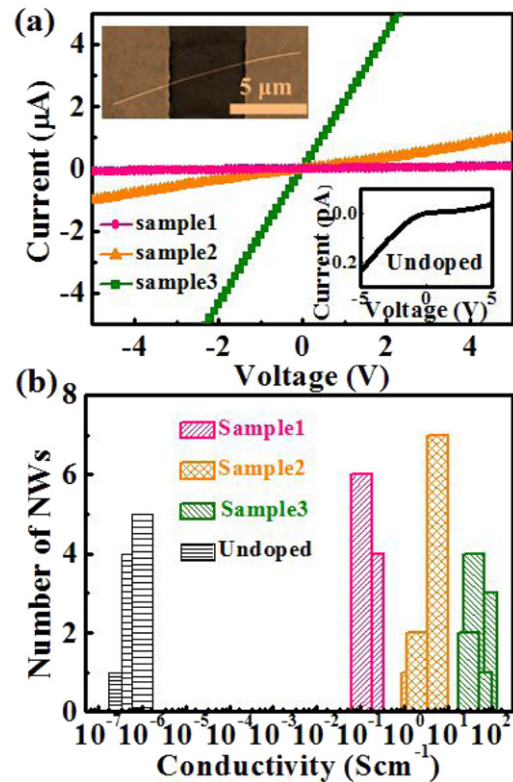


Figure 3. (a) I - V curves of ZnSe:Sb NWs with varied doping levels in the dark. The lower right inset shows the I - V curve of an undoped ZnSe NW, the upper left inset shows a representative SEM image of a single ZnSe NW connected by two parallel Cu/Au electrodes. (b) Conductivity histogram for four kinds of samples, 10 NWs for each sample; the measurements were all carried out in the dark.

10^{19} cm^{-3} from $\rho = 1/\sigma = 1/nq\mu$. Similar p-type operating characteristics were observed on FET devices made from samples 2 and 3 as well. Analogous analysis of I - V data leads to transconductances of 2.66 and 17.50 pS and a hole mobilities of 2.19×10^{-1} and $1.52 \text{ cm}^2 \text{ V}^{-1} \text{ s}^{-1}$ for samples 2 and 3, respectively (figures 4(c) and (d)). The moderate increase in hole mobility with increasing doping level is possibly associated with the change of semiconductor/metal contact barrier. The key device parameters of the ZnSe:Sb NW FETs with varied doping levels are summarized in table 1, according to which it is found that with increase of Sb content in ZnSe NWs, the transconductance, conductivity, hole mobility and concentration are all improved considerably. It is worth mentioning that the conductivity of the p-type ZnSe:Sb NWs is about 2–3 orders of magnitude larger than those of ZnSe:As and ZnSe:Bi NWs [24, 25]. More importantly, the activation of doped atoms can be conveniently achieved without resorting to post-treatment such as fast annealing, suggesting that the Sb atom is a very efficient dopant for p-type doping of ZnSe NWs.

In order to explore the potential for device applications, p-type NWs from sample 3 together with n-type ZnO:Ga were used to assemble complementary crossed p-n nanostructures. The scheme in figures 5(a)–(d) schematically illustrates the flow chart to fabricate a p-ZnSe:Sb NW/n-ZnO:Ga NW junction. Briefly, the Ga doped ZnO NW was first dispersed

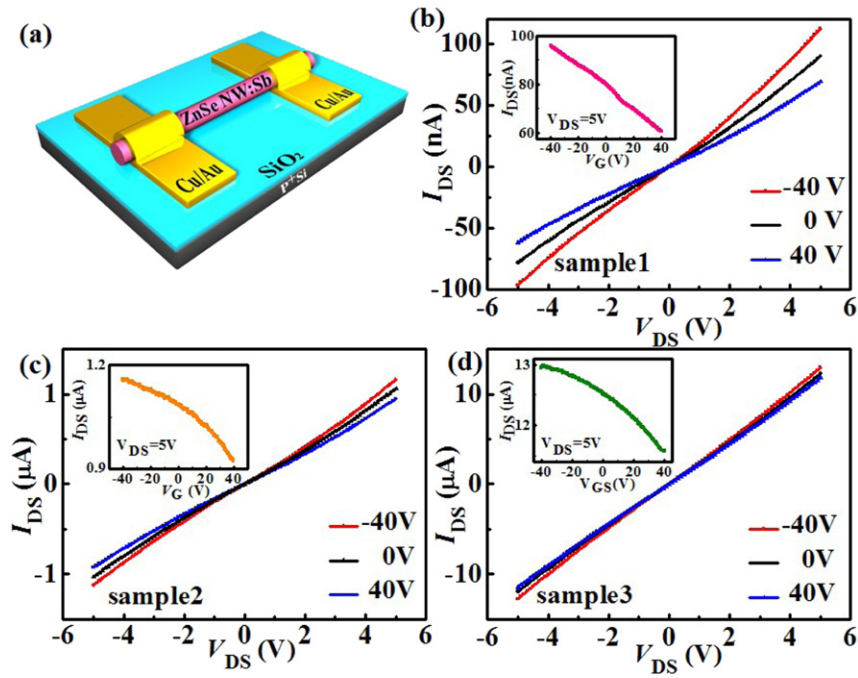


Figure 4. (a) Schematic illustration of the back-gate ZnSe NW metal–oxide field-effect-transistor. Electrical transfer characteristics of ZnSe:Sb NWs with different doping levels. (b)–(c) I_{DS} – V_{DS} curves of sample 1 (b), sample 2 (c) and sample 3 (d). All insets show the corresponding I_{DS} – V_{GS} curves at $V_{DS} = 5$ V.

Table 1. Summary of the key device parameters of the FETs based on ZnSe:Sb NWs with different doping levels.

Sample No.	Doping density (%)	g_m (ns)	σ (S cm $^{-1}$)	μ_p (cm 2 V $^{-1}$ s $^{-1}$)	p (10 19 cm $^{-3}$)
Undoped	0	—	6.36×10^{-7}	—	—
1	0.2	0.385	0.28	3.18×10^{-2}	5.50
2	1.2	2.660	3.32	2.19×10^{-1}	9.47
3	2.3	17.50	37.33	1.52	15.30

on a SiO $_2$ (300 nm)/p $^+$ -Si substrate; two Ti electrode contacts (70 nm) were then deposited on the ZnO NW. To form the crossed contact, a ZnSe:Sb NW was then mechanically transferred across the ZnO NW using a contact printing technique [30], followed by deposition of a copper–gold electrode (4 nm Cu/70 nm Au). An SEM image of the p–n junction device is shown in figure 5(e). For the sake of convenience, the two electrodes connecting the ZnO NW are defined as ‘1’ and ‘2’, while the two electrodes connecting the ZnSe NW are defined as ‘3’ and ‘4’ (figure 5(d)).

Figure 6(a) shows the I – V characteristics of the crossed hetero-junction diode. Obviously, the junction exhibits distinctive rectification behavior which is characteristic of a p–n junction. Specifically, little current (less than 6 nA) is observed at a reverse bias of -5 V. The current begins to increase dramatically at a forward bias of ~ 0.9 V. Moreover, the forward current (I_F) of the junction at 5 V is 4.3 μ A, while the reverse leakage current (I_R) at -5 V bias is less than 4.13 nA, yielding a rectification ratio (I_F/I_R) as great as 10^3 at ± 5 V. For such a p–n junction diode, the rectification curve can be expressed using the following equation:

$$I_{pn} = I_0(e^{V_{pn}/nKT} - 1). \quad (2)$$

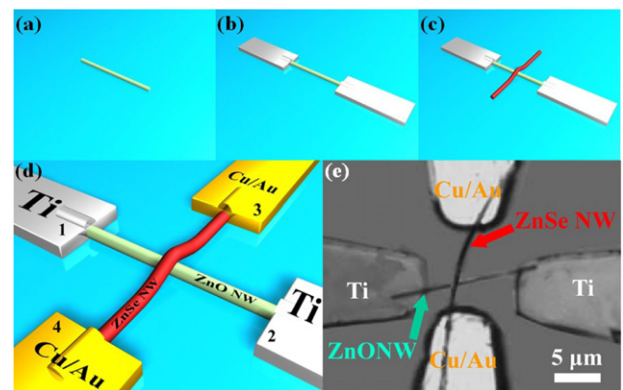


Figure 5. (a)–(d) Schematic illustration of the step-wise process for the fabrication of a ZnSe:Sb NW/ZnO:Ga NW p–n junction. (e) A typical SEM image of the p–n junction device.

In equation (2), the ideality factor n can be described by

$$n = \frac{q}{KT} \frac{dV_{pn}}{d \ln I_{pn}}, \quad (3)$$

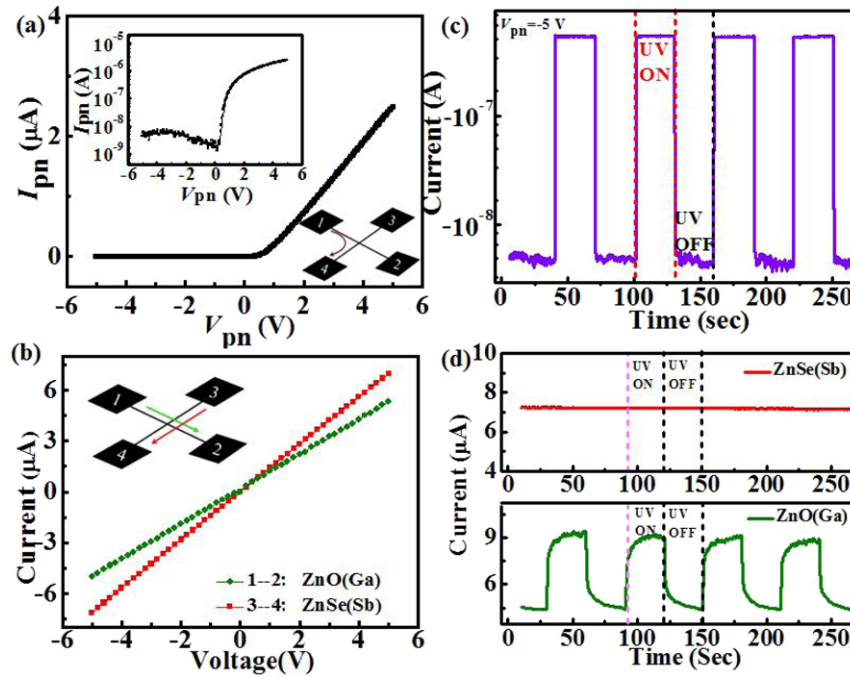


Figure 6. (a) The I - V characteristics of the crossed p - n junction measured at ambient conditions in the dark; the upper left inset shows the semi-log plot of the rectifying curves and the lower right inset shows the testing mode (1-4). (b) The I - V characteristics of the individual ZnO NW (1-2) and the ZnSe NW (3-4). (c) The photoresponse of the p -ZnSe:Sb NW/ n -ZnO:Ga junction diode (1-4) under illumination with 365 nm UV light. (d) The photoresponse of the single ZnO:Ga NW (1-2) and the ZnSe:Sb NW (3-4) under illumination with 365 nm UV light. During the photodetection measurement, the light intensity and the bias voltage were kept at $100 \mu\text{W cm}^{-2}$ and -5 V , respectively. The UV light was switched on and off manually.

where I_0 is the reverse bias leakage current and K and T are the Boltzmann constant and the temperature in kelvins, respectively. By fitting the rectification curve, a value of $n = 1.88$ was obtained. This ideality factor is larger than unity, and can be ascribed to the series resistance and various defects as a result of the lattice mismatch between the ZnSe:Sb and ZnO:Ga NW interfaces [31]. To unveil the origin of these current rectification characteristics, the contacts of both doped n -type ZnO:Ga NW/Ti and p -type ZnSe:Sb NW/Cu:Au were also analyzed. Figure 6(b) shows the I - V data recorded from electrodes '1'-'2' and '3'-'4', from which two linear and symmetric curves were observed. This result suggests that very good contact (Ohmic contact) without any barriers was formed at the semiconductor/metal interfaces. Thus, it can be concluded that the observed rectifying behavior is due to the crossed p -type ZnSe:Sb NW/ n -type ZnO:Sb NW contact.

Notably, when it was illuminated with UV light from a Hg lamp (wavelength: 365 nm), the crossed ZnSe:Sb NW/ZnO:Ga NW junction displayed pronounced photoresponse. Figure 6(c) shows the time photoresponse measured at room temperature under illumination. It is seen that the electrical current increased sharply and stabilized in a high-conduction state upon light radiation, but it decreased quickly to a low-conduction state after the UV light was turned off, with very good stability and reproducibility. The current on/off ratio was as high as 60. It should be noted that the performance of the p - n junction diode is superior to that of photoconductive type PDs solely composed of ZnO NW or ZnSe NWs (figure 6(d)). The cause of the weak or

blind photoresponse of ZnO or ZnSe NWs is probably the short carrier lifetime of the photogenerated minority, as a consequence of the presence of a huge amount of deep level impurities that can act as effective recombination centers. In addition to the relatively large on/off ratio, careful analysis of the crossed junction device also reveals a rise and fall time of less than 1.0 s, much quicker than that of a UVPD solely made of a single ZnO:Ga NW. This quick photoresponse is probably due to the unique working mechanism, as will be discussed later.

To evaluate the device performance in a more quantitative way, the responsivity (R), gain (G) and detectivity (D^*), three essential parameters reflecting the sensitivity of a UVPD to incident light, were calculated. For the crossed p -ZnSe:Sb NW/ n -ZnO:Ga NW junction UVPD, the three parameters can be expressed as [32, 33]:

$$R (\text{A W}^{-1}) = \frac{I_1 - I_d}{P_{\text{opt}}} = \eta \left(\frac{q\lambda}{hc} \right) G, \quad (4)$$

$$G = \frac{N_{\text{el}}}{N_{\text{ph}}} = \frac{\tau}{\tau_{\text{tr}}}, \quad (5)$$

$$D^* = \sqrt{\frac{A}{2qI_d}} R, \quad (6)$$

where I_1 is the photocurrent, I_d is the dark current, P_{opt} is the incident light power, η is the quantum efficiency, h is Planck's constant, c is the speed of light, λ is the incident light wavelength, A is the area of the UVPD and q is the

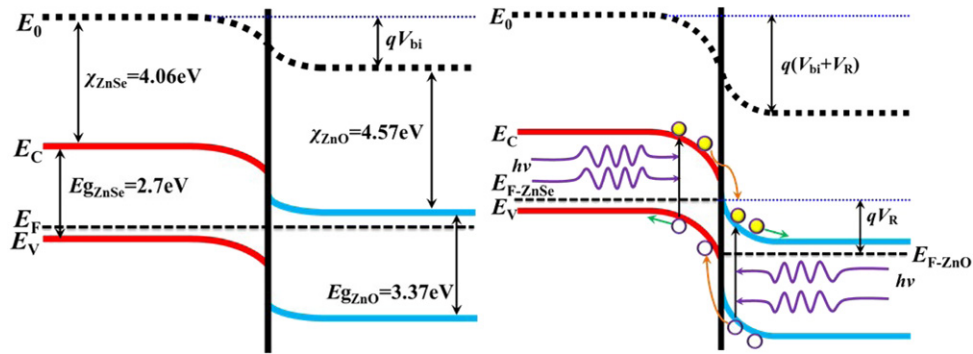


Figure 7. (a) Energy diagrams of the ZnSe:Sb NW/ZnO:Ga NW p-n hetero-junction UVPD at zero bias (a) and reverse bias (b).

Table 2. A summary of the performance of the ZnSe:Sb NW/ZnO:Ga NW UVPD. Values from previous reports are also provided for comparison.

Materials	Responsivity (R) ($A W^{-1}$)	Gain (G)	Detectivity (D^*) ($cm Hz^{1/2} W^{-1}$)
This work	5.2×10^5	1.77×10^6	5.5×10^{14}
ZnO NW [36]	≈ 0.055	$\approx 10^2$	7.43×10^{11}
ZnS:Al NW [37]	8.8×10^5	4.3×10^6	—
ZnS:Cl NW [32]	8.2×10^5	4.0×10^6	—
ZnSe [38]	—	—	1.4×10^{10}
ZnTe NW [39]	2.2×10^3	1.5×10^4	—
ZnTe:Sb NR [40]	4.8×10^4	1.2×10^5	4.8×10^{13}
ZnTe:Sb NR/Si [40]	1.8×10^3	4.2×10^3	—
CdS NR [41]	$\approx 10^4$	100	—
CdSe NW [42]	10–100	0.05	—

charge of an electron. Physically, the photoconductive gain (G) is defined as the ratio between the number of electrons collected per unit time (N_{e1}) and the number of absorbed photons per unit time (N_{ph}), or the ratio of carrier lifetime (τ) to carrier transit time (τ_{tr}). The detectivity (D^*) represents the normalized radiation power required to give a signal from a photoconductor that is equal to the noise. Assuming $\eta = 1$ for simplification, R , G and D^* are estimated to be $5.2 \times 10^5 A W^{-1}$, 1.77×10^6 and $5.5 \times 10^{14} cm Hz^{1/2} W^{-1}$, respectively (cf the supporting information available at stacks.iop.org/Nano/24/095603/mmedia). Table 2 lists these key parameters from this work and other semiconductor nanostructure based UVPDs. To the best of our knowledge, the detectivity is the largest ever reported. Moreover, the responsivity and detectivity of our device are comparable to those of ZnS:Al and ZnS:Cl NW based UVPDs, but much higher than those of UVPDs assembled from ZnO, ZnTe and ZnTe:Sb NWs and visible light PDs from CdS and CdSe NWs. Although the underlying reason for the very high responsivity, gain and detectivity is not clear at this stage, we think that the following factors are the possible reasons. (1) The novel device configuration of the p-n nano-junction diode. Our crossed device is largely relying on a tiny contact with an area of less than $10^{-8} cm^2$, in contrast to traditional nanostructure based UVPDs in which a relatively long nanowire or a nanoribbon with a relatively large working area is employed. This feature makes it possible to detect UV irradiation with high sensitivity. (2) The long photogenerated minority

carrier mean lifetime. As we will discuss later, electron-hole pairs will be efficiently separated by the large electric field formed at the space charge region. As a result, the carrier lifetime is greatly prolonged due to reduced electron-hole recombination.

Unlike the traditional single NW based photoconductive type UVPD [34], our crossed junction UVPD is capable of detecting UV light illumination in a different way. Figures 7(a) and (b) illustrate the energy band diagrams of the p-n hetero-junction diode at both zero and reverse biases. As a result of the difference in energy levels, a built-in electric field (V_{bi}) with the direction ZnO NW to ZnSe NW is formed at the interface. When the diode is reverse biased, namely, a positive value of V_R is added to V_{bi} , the UVPD will have a depleted region with a high electric field which serves to separate the photogenerated electron-hole pairs very efficiently (figure 7(b)). Upon incident UV light (365 nm) illumination, a tremendous amount of electron-hole pairs on both the ZnSe:Sb NW and ZnO:Ga NW sides will be generated. When the electron-hole pairs diffuse to the interface of the NWs, they will be separated by the huge built-in electric field ($V_{bi} + V_R$) and immediately collected by the electrodes. These carriers continued to drift and finally form the photocurrent in the circuit [35]. When the light is turned off, the photogenerated minority carrier drops sharply and the diode shuts off under reverse bias, thus the photocurrent disappears very quickly.

4. Conclusion

In summary, we have presented the large-scale synthesis of p-type ZnSe NWs by using a simple thermal evaporation method, in which Sb powder was used as the dopant. Structural characterization indicated that the as-obtained ZnSe NWs were of single-crystal type, with growth orientation along the [001] direction. Electrical analysis of the Sb-doped ZnSe nanowires revealed that by increasing the Sb content in the source materials from 0.5, to 5, to 10%, controllable p-type ZnSe NWs could be readily achieved, with the conductivity increasing from ~ 0.28 , to 3.32, to 37.3 S cm^{-1} . In addition, a crossed p-n junction diode was assembled from the as-doped ZnSe:Sb NW and ZnO:Ga NW. It was observed that the device exhibited distinctive rectification behavior, with a rectification ratio as high as 10^3 at $\pm 5 \text{ V}$. Remarkably, in reverse bias, it was highly sensitive to 365 nm ultraviolet (UV) light irradiation, with a response time of less than 1 s. It is anticipated that these ZnSe:Sb NW building blocks will open up significant potential for the assembly of nanoscale optoelectronic devices.

Acknowledgments

The authors acknowledge the financial support of the National Natural Science Foundation of China (Nos 60806028, 61106010, 21101051 and 20901021), the Fundamental Research Funds for the Central Universities (2012HGXC0003) and the Major Research Plan of the National Natural Science Foundation of China (No. 9102702).

References

- [1] Iijima S 1991 *Nature* **354** 56
- [2] Li Y, Qiang F, Xiang J and Lieber C M 2006 *Mater. Today* **9** 18
- [3] Hu Z Z, Zhang X J, Xie C, Wu C Y, Zhang X Z, Bian L, Wu Y M, Wang L, Zhang Y P and Jie J S 2011 *Nanoscale* **3** 4798
- [4] Cui Y, Wei Q, Park H and Lieber C M 2001 *Science* **293** 1289
- [5] Luo L B, Yang X B, Liang F X, Jie J S, Wu C Y, Wang L, Yu Y Q and Zhu Z F 2011 *J. Phys. Chem. C* **115** 49
- [6] Qian E, Li Y, Gredecak S, Wang D, Barrelet C J and Lieber C M 2004 *Nano Lett.* **4** 1975
- [7] Dejarld M, Shin J C, Chem W, Changda D, Balasundaram K, Rogers J A and Li X L 2011 *Nano Lett.* **11** 5259
- [8] Ma R M, Dai L and Qin G G 2007 *Nano Lett.* **7** 868
- [9] Xie X *et al* 2012 *Nanoscale* **4** 2914
- [10] Luo L B, Yang X B, Liang F X, Jie J S, Li Q, Zhu Z F, Wu C Y, Yu Y Q and Wang L 2012 *CrystEngCommun.* **14** 1942
- [11] Qian H S, Yu S H, Gong J Y, Luo L B and Fei L F 2006 *Langmuir* **22** 3830
- [12] Xia Y N, Yang P D, Sun Y G, Wu Y Y, Mayers B, Gates B, Yin Y D, Kim F and Yan H Q 2003 *Adv. Mater.* **15** 353
- [13] Duan X F, Huang Y, Agarwal R and Lieber C M 2003 *Nature* **421** 241
- [14] Jie J S, Zhang W J, Bello I, Lee C S and Lee S T 2010 *Nano Today* **5** 313
- [15] Xie C *et al* 2012 *CrystEngCommun.* **14** 7222
- [16] Zhai T Y, Fang X S, Li L, Bando Y and Golberg D 2010 *Nanoscale* **2** 168
- [17] Gul S, Cooper J K, Corrado C, Vollbrecht B, Bridges F, Guo J H and Zhang J Z 2011 *J. Phys. Chem. C* **115** 20864
- [18] Fang X S, Xiong S L, Zhai T Y, Bando Y, Liao M Y, Gautam U K, Koide Y, Zhang X G, Qian Y T and Golberg D 2009 *Adv. Mater.* **21** 5016
- [19] Salfi J, Philipose U, Sousa C F D, Aouba S and Ruda H E 2006 *Appl. Phys. Lett.* **89** 261112
- [20] Wang Z *et al* 2012 *Chem. Plus. Chem.* **77** 470
- [21] Wang L *et al* 2012 *Sci. Adv. Mater.* **4** 332
- [22] Lei M, Fu X L, Yang H J, Wang Y G, Li P G, Hu Q R and Tang W H 2012 *Mater. Chem. Phys.* **133** 823
- [23] Davies J J, Wolverson D, Aliev G N, Zeng S, Wang J F and Isshiki M 2003 *Semicond. Sci. Technol.* **18** 978
- [24] Zhang X W, Jie J S, Wang Z, Wu C Y, Wang L, Peng Q, Yu Y Q, Jiang P and Xie C 2011 *J. Mater. Chem.* **21** 6736
- [25] Song H S, Zhang W J, Yuan G D, He Z B, Zhang W F, Tang Y B, Luo L B, Lee C S, Bello I and Lee S T 2009 *Appl. Phys. Lett.* **95** 033117
- [26] Xu C X, Sun X W and Chen B J 2004 *Appl. Phys. Lett.* **84** 1540
- [27] Zhu Y C and Bando Y 2003 *Chem. Phys. Lett.* **377** 367
- [28] Jiang Y, Meng X M, Yiu W C, Liu J, Ding J X, Lee C S and Lee S T 2004 *J. Phys. Chem. B* **108** 2784
- [29] Zhu L, Jie J S, Wu D, Luo L B, Wu C Y, Zhu Z F, Yu Y Q and Wang L 2012 *J. Nanoeng. Nanomanuf.* **2** 191
- [30] Fan Z Y, Ho J C, Takahashi T, Yerushalmi R, Takei K, Ford A C, Chueh Y L and Yavey A 2009 *Adv. Mater.* **21** 3730
- [31] Roy S, Jacob C and Basu S 2004 *Solid State Sci.* **6** 377
- [32] Yu Y Q *et al* 2011 *J. Mater. Chem.* **21** 12632
- [33] Liu J M 2005 *Photonic Devices* (New York: Cambridge University Press)
- [34] Luo L B, Liang F X and Jie J S 2011 *Nanotechnology* **22** 485701
- [35] Sze S M 2008 *Semiconductor Devices: Physics and Technology* (New York: Wiley)
- [36] Chang S P, Lu C Y, Chang S J, Chiou Y Z, Hsueh T J and Hsu C L 2011 *IEEE J. Sel. Top. Quantum Electron.* **17** 990
- [37] Jiang P, Jie J S, Yu Y Q, Wang Z, Xie C, Zhang X W, Wu C Y, Wang L, Zhu Z F and Luo L B 2012 *J. Mater. Chem.* **22** 6856
- [38] Vigue F, de Mierry P, Faurie J P, Monroy E, Calle F and Munoz E 2000 *Electron. Lett.* **36** 826–7
- [39] Cao Y L, Liu Z T, Chen L M, Tang Y B, Luo L B, Jie J S, Zhang W J, Lee S T and Lee C S 2011 *Opt. Express* **19** 6100
- [40] Wu D *et al* 2012 *J. Mater. Chem.* **22** 6206
- [41] Jie J S, Zhang W J, Jiang Y, Meng X M, Li Y Q and Lee S T 2006 *Nano Lett.* **6** 1887
- [42] Kung S C, van der Veer W E, Yang F, Donovan K C and Penner R M 2010 *Nano Lett.* **10** 1481